Expanded graphite – paraffin composite phase change materials

Zhao, Yanqi; Jin, Lu; Zou, Boyang; Qiao, Geng; Zhang, Tongtong; Cong, Lin; Jiang, Feng; Li, Chuan; Huang, Yun; Ding, Yulong

DOI:
10.1016/j.applthermaleng.2020.115015

Document Version
Peer reviewed version

Citation for published version (Harvard):
Zhao, Y, Jin, L, Zou, B, Qiao, G, Zhang, T, Cong, L, Jiang, F, Li, C, Huang, Y & Ding, Y 2020, 'Expanded graphite – paraffin composite phase change materials: effect of particle size on the composite structure and properties', *Applied Thermal Engineering*, vol. 171, 115015, pp. 1-12. https://doi.org/10.1016/j.applthermaleng.2020.115015

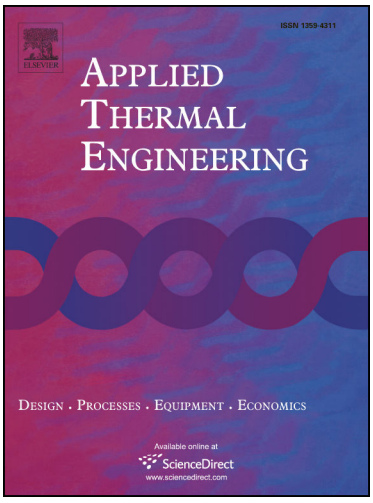

Expanded Graphite – Paraffin Composite Phase Change Material: Effect of Particle Size on the Composite Structure and Properties

Yanqi Zhao, Lu Jin, Boyang Zou, Geng Qiao, Tongtong Zhang, Lin Cong, Feng Jiang, Chuan Li, Yun Huang, Yulong Ding

PII: S1359-4311(19)37301-6
DOI: https://doi.org/10.1016/j.applthermaleng.2020.115015
Reference: ATE 115015

To appear in: *Applied Thermal Engineering*

Received Date: 22 October 2019
Revised Date: 17 January 2020
Accepted Date: 26 January 2020

Please cite this article as: Y. Zhao, L. Jin, B. Zou, G. Qiao, T. Zhang, L. Cong, F. Jiang, C. Li, Y. Huang, Y. Ding, Expanded Graphite – Paraffin Composite Phase Change Material: Effect of Particle Size on the Composite Structure and Properties, *Applied Thermal Engineering* (2020), doi: https://doi.org/10.1016/j.applthermaleng.2020.115015

Expanded Graphite – Paraffin Composite Phase Change Material: Effect of Particle Size on the Composite Structure and Properties

[a]Yanqi Zhao, [b]Lu Jin, [a]Boyang Zou, [b]Geng Qiao, [a]Tongtong Zhang, [a]Lin Cong, [a]Feng Jiang, [a]Chuan Li, [c]Yun Huang and [a*]Yulong Ding

[a]*Birmingham Centre for Energy Storage & School of Chemical Engineering, University of Birmingham, Birmingham B15 2TT, United Kingdom*

[b]*Global Energy Interconnection Research Institute Europe, Berlin, Germany*

[c]Institute of Process Engineering, Chinese Academy of Sciences, Beijing 100080, China

**Corresponding author: y.ding@bham.ac.uk*

Abstract

Expanded graphite (EG) is highly thermally conductive and has a porous structure, making it an ideal candidate for shape stabilisation of phase change materials (PCMs). We investigated the effect of EG size on the structure and properties of EG based paraffin composite PCMs for which no reports have been found in the literature. Large EG particles have a loose vermicular shape with a significant number of pores and voids in irregular shapes and varied sizes, which links together form a strong networking structure. A higher degradation temperature with up to 31 °C increase was observed for the composite phase change material (CPCM) containing large EG particles, which also showed a significant level of thermal conductivity enhancement of up to 1695% compared with the paraffin. Phase change temperature hysteresis between the melting and solidification temperature was observed on the CPCM using large EG particles. Higher loading of the EG reduced the temperature hysteresis mainly due to a higher heat transfer rate. Fine EG particles are primary in the form of loose graphite sheets. The structural defect gave worse thermal cycling stability to the composite containing fine EG particles than the composites using large EG particles. The CPCM made from fine EG particles also has a significantly higher thermal degradation temperature with up to 37 °C increase partially due to the existence of interfacial thermal resistance but gives a low level of thermal conductivity enhancement of up to 340%.

Keywords: expanded graphite; phase change material; composite; particle size effect; composite structure; thermal conductivity

1. Introduction

Organic low-molecular PCM paraffin is a promising candidate for thermal energy storage (TES) due to the high latent heat, good thermal reliability, low volume change during phase transition and low supercooling degree [1]. However, pure paraffin has a low thermal conductivity of roughly 0.2 W/mK. In order to improve the thermal conductivity of pure PCM, various thermal conductive materials have been investigated, including impregnating expanded graphite (EG) matrix into PCM [2], saturating aluminium foam with PCM [3], dispersing carbon fibre into PCM [4] and applying PCM with aluminium wire mesh [5].

Among all the materials, carbon-based nanomaterials have been proved to be excellent choices due to their high thermal conductivity and good compatibility with organic PCMs. Ramakrishnan [6] enhanced the thermal conductivity of paraffin/hydrophobic expanded perlite composites with graphite, carbon nanotube and graphene nanoplates. Results showed that addition of 0.5wt% carbon-based material can improve the thermal conductivity with 30% to 49%. Sari et al. [7,8] investigated thermal property enhancement ability of carbon nanotube. The researchers found that when 1wt% and 2.5wt% of carbon nanotube were added into polyethene glycol/raw diatomite composite and myristic acid/silica fume composite, the thermal conductivity can be improved by and 43.8% and 93%, respectively.

EG is another promising carbon-based material with excellent thermal property and cost advantage. The porous material has pores and voids which is consisted of many large and thin graphite flakes. The graphite flakes have high in-plane thermal conductivity and it provides EG with high thermal conductivity [9]. The capillary forces of the pores and voids in EG can pull PCM into the matrix. In this way, it confines the PCM in the pores and voids and increases the thermal conductivity of the composite [10]. Karaipekli et al. [11] improved the thermal conductivity of stearic acid using EG. Results showed a linear relationship between the thermal conductivity and mass fraction of EG, with 10% of EG the thermal conductivity was increased by 266.6% and reached 1.1 W/mK. Sari et al. [12] developed a novel palmitic acid/EG composite with excellent thermal stability. FTIR results confirmed that after 3000 times of thermal cycling the chemical structure of the composite material remains the same. DSC results also showed that change of melting and solidification temperature and latent heat of the composites were at an acceptable level. Sari et al. [13] also studied the paraffin/EG composite material and found that with 10 wt% EG the thermal conductivity of the composite was measured to be 0.82 W/mK. Zhang et al. [14] investigated the flammability of

EG/paraffin/high-density polyethene composites. The results showed that flame retardancy of the composite can be improved with the existence of EG, as EG could form a char layer with good strength and stability under heating.

The thermal property of CPCM is affected by the particle size of the supporting material. For particulate composites, if the particle is too small, interfacial thermal resistance dominates the influence on thermal conductivity of the composite. If the particle size is relatively large, the thermal conductivity of the composites is decided by the bulk property [15]. Chirtoc et al. [9] investigated the role of particle size and interfacial thermal resistance in determining the thermal conductivity enhancement ability of EG. The authors found that a large particle size leads to high thermal conductivity enhancement. When the particle size of EG is lower than the threshold (Kapitza radius), the interfacial thermal resistance will reduce the thermal conductivity enhancement. Luo et al. [16] studied the effect of particle size on the thermal transport between graphene and paraffin numerically. The researchers concluded that elongating graphene flake could enhance the thermal transport hence improving the thermal conductivity of the composite. Every et al. [17] observed that thermal conductivity of ZnS was improved when large particle size diamond was added but lowered by adding sub-micron size particles of the diamond. The authors proposed a theory as interfacial thermal resistance becoming dominant when the particles become small.

When confined in pores and voids of EG, PCM exhibits different phase change behaviour from the bulk PCM and a shift on the phase change temperature of the PCM will happen. The shift of the melting and freezing temperatures was explained by the Clapeyron–Clausius equation, as the enthalpy and volume of the PCM changes during the phase change. The change on the phase change behaviour could also be due to the interaction between the PCM surface and the pore surface [18,19]. Pore structure could also be the reason which causes the change in the phase change temperature. According to Awschalom and Warnock's research [20], the geometry of the PCM changes when confined in pores, leading to different property unlike that of pure PCM. It causes the observed increase in hysteresis.

Through literature review, it was found that researches on the effect of particle size on the thermal property of the composite have also been inadequate. Besides many present studies of EG/composite material neglect the temperature hysteresis between the PCM and EG/PCM composites. When confined in EG, PCM was believed to have little or no change in the phase change temperature. The shift of melting and solidification temperature of the PCM could

cause problems in the real application as it will cause deviations from the expected working temperature. In the current research, composites with different particle sizes of EG and different mass fractions of EG were prepared. In order to study the effect of particle size on the thermal property, the prepared materials were examined in terms of surface morphology and 3D structure using scanning electron microscope (SEM) and X-ray nano-ct system (XRT), respectively, and thermal property and thermal stability were studied by differential scanning calorimetry (DSC), laser flash apparatus (LFA) and simultaneous thermal analyser (STA).

2. Experimental

2.1 Material

Table 1 Physical properties of the raw material (RT 28HC)

Physical property	Parameter
Peak Melting temperature（°C）	28.02
Peak Solidification temperature （°C）	26.24
Specific heat（kJ/kg·K）	2
Latent heat (kJ/kg）	220
Density（Liquid）（kg/m^3）	0.77
Density（Solid）（kg/m^3）	0.88
Flash point（°C）	165

Paraffin (RT28HC) was purchased from Rubitherm as the phase change material for this study, characteristics of the PCM were listed in Table 1 (the property was supplied by Rubitherm). Three EG with different particle size were purchased from Donghai Anfa International trade company Ltd. EG1 and EG2 were in large micrometres scale (i.e. hundreds μm), while particles of EG3 were in lower micrometres scale (i.e. below 10 μm). EG particles were sieved first using sieves with different sizes. The size of the EG particles was then verified using SEM, their dimensional information is given in Table 2.

Table 2 Particle size of different EGs

Type of EG	Diameter/width (μm)	Length (μm)
EG1	400	1000
EG2	120	200
EG3	Less than 1	10

2.2 Preparation of EG/paraffin composites

Shape stabilized PCM composites were prepared by physical blending and impregnating of the PCM into different EGs. Paraffin was pre-melted using a magnetic hotplate stirrer. Then EG was slowly added to the melted paraffin with continuous stirring. The mixture was stirred for 10 minutes to ensure the homogeneity of the mixture. Next, the mixture was transferred into an ultrasonic water bath to accelerate the impregnation of liquid paraffin. After the impregnation, the surface of EG was coated with paraffin and the pores of the EG were filled with paraffin. The prepared sample was then cooled at room temperature and compacted using a Lloyd LS100 Plus materials testing machine. Samples were compressed into a solid matrix with a flat cylindrical shape. The process of sample preparation is illustrated in Figure 1.

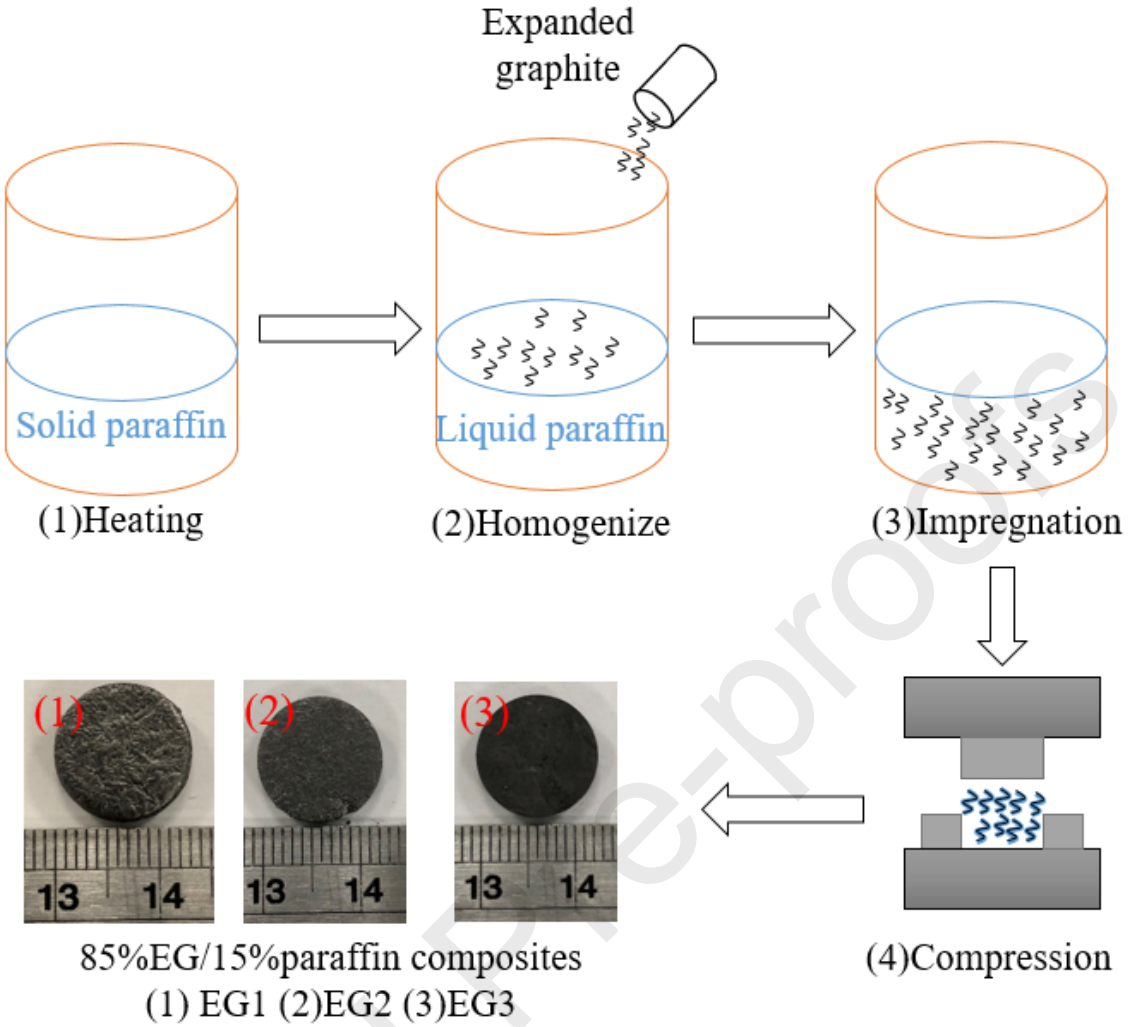

Figure 1 the process of the CPCM sample preparation.

The samples were weighed within the error of ± 0.1mg. The prepared samples have the same weight of 0.24g, 13mm in diameter and roughly 3mm in height. All samples should have the same density as this property is directly related to the thermal conductivity and porosity estimation of composites. Wang et al. found out that increased compression pressure on expanded graphite will cause the change of thermal conductivity and permeability [21]. Because the selected EGs possess different density initially, thus the compression strength was ranging from 0.2 to 30KN to attain a similar density of final composites. During the compression, no leakage of paraffin was observed which indicated the sufficient adsorption of the paraffin. Composites were prepared with paraffin and different particle size of EG, with the EG mass ratio in 5% increments from 15% to 25%.

2.3 Characterization of EG/paraffin composite

The surface morphology of EG and paraffin/EG composites were observed using a scanning electronic microscope (SEM, HITACHI Microscope TM3030). The observations were performed at different magnifications with different acceleration voltages.

Nano-CT system (XRT, Bruker SKYSCAN 2211) was used to attain the porosity information of paraffin/EG composites. XRT is a non-destructive technique wherein thousands of 2D raw images are acquired from different angular positions of the composite. Using the 2D reconstructed images of the samples will be able to build a 3D volume rendering which enables to reveal the impregnated PCM in EG matrixes. The 3D model gives the structure parameter of the EG matrix and distribution condition of the PCM. Flat-panel X-ray detector was used, and 1200 images were generated with the scanning step angle of 0.3°. In order to obtain the structure parameters from the 3D models, VOI (volume of interest) needs to be carefully defined firstly. It refers to the sub-volume of the dataset within which EG matrix is exactly included. The images also need to be segmented, i.e. to confirm the suitable grey level (0-255) threshold. Same segmentation method was applied to all the samples. After segmentation, voxels that reprsent the porosity were efficiently distinguished from the EG constituent. An example of the 3D binary XRT image and the grey level frequency histogram after segmentation is shown in Figure 2. The specific surface area was defined as the object surface area per object volume space. Pore volume is the difference between the VOI and the EG matrix volume. The porosity was calculated as follows:

$$\%\text{Porosity} = 1 - \frac{EG\ matrix\ volume}{VOI\ volume}$$

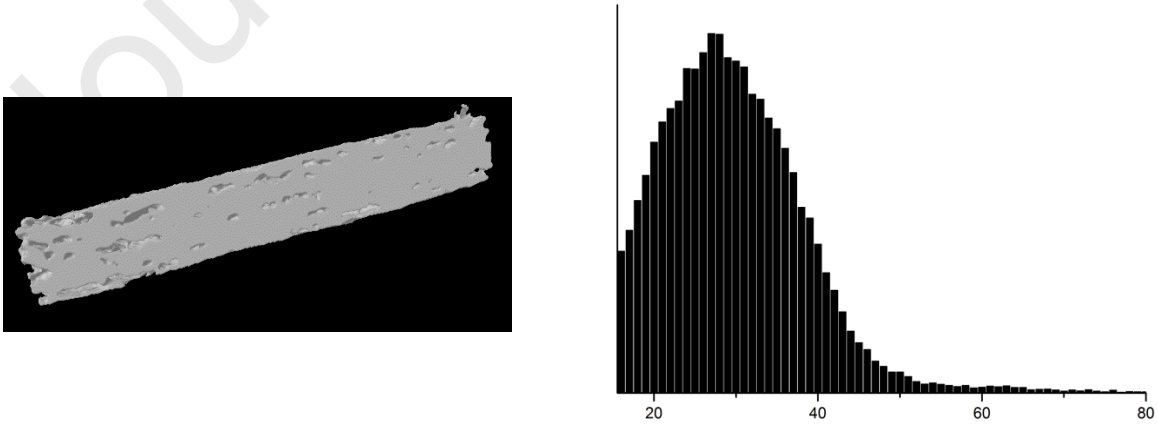

Figure 2 One of the Cut surface of the EG1 3D binary image (Left), selected grey level of the image (right).

Thermal properties of paraffin/EG composites, such as latent heat, specific heat, melting and solidification temperature, were measured by differential scanning calorimeter (DSC, Mettler Toledo DSC 3). The tests were performed in a nitrogen atmosphere from 0 to 50 °C and 50 to 0 °C at a heating/cooling rate of 5 °C/min. Samples were weighted using a high precision balance (Mettler Toledo XP6U Micro Comparator) with the readability of 0.0001 mg. The weight of the samples was controlled in the range of 3-6mg. All samples were tested under three heating and cooling cycles. Specific heat was measured using the sapphire method according to DIN 51007 [22]:

$$C_p = \frac{(\Phi_{meas} - \Phi_{bl})}{m_{sam}} * \frac{m_{sap}}{(\Phi_{sap} - \Phi_{bl})} * C_{p.sap}$$

where m_{sap} and $C_{p.sap}$ are known that represent the weight and specific heat of the sapphire, respectively. Φ_{sap} and Φ_{bl} denote the heat flow applied on the sapphire and blank, respectively. Φ_{meas} is the measured total heat flow and m_{sam} is the measured sample weight.

Thermal conductivities of EG/paraffin composites were measured by Laser Flash Apparatus (LFA, NETZSCH LFA 427). The measurements were performed under a nitrogen atmosphere from 30 to 70 °C with a measurement interval of 10°C. At each temperature set point, the measurement was repeated five times in order to ascertain the correct values.

The thermal stability of materials was characterized by a simultaneous thermal analyser (STA, NETZSCH STA 449 F3 Jupiter) from 25 °C to 400 °C with a heating rate of 10°C/min. Leakage phenomenon was also studied by comparing the weight of the samples before and after cycling. The samples were cycled between 15 and 45 °C for 50 times and weight loss were calculated according to the following equation [23] :

$$\text{weight loss}\% = 100 - \frac{(m_{before} - m_{after})}{m_{before} * w} * 100$$

where m_{before} is the weight of the sample before cycling, m_{after} is the weight of the sample after cycling, w is the mass fraction of the paraffin.

3. Results and Discussions

3.1 Microstructure of the composites

3.1.1 Morphology observation

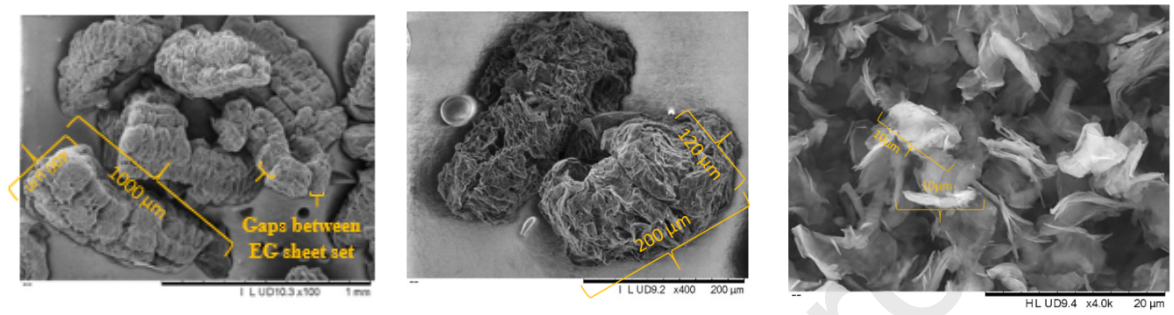

(a) ~ 400 *1000 µm (w*l) (b) ~ 120 * 200 µm (w*l) (c) ~ <1 * 10 µm (w*l)

Figure 3 Particle size observation of different EG particles: (a) EG1, (b) EG2, (c) EG3

Particles size of the EG particles were examined and confirmed through SEM imaging on different samples. Figure 3 shows SEM images of the purchased EGs (more pictures see in supplementary material). A distinct difference in the morphology was observed between EG3 and the other two EGs. EG1 and EG2 were in large micrometres scale with the loose vermicular shape. On the surface of EG1, sets of graphite sheets were arranged in parallel, gaps with an approximate size of (30µm*200 µm) in between each graphite sheet set. Whereas EG3 with the micro-scale presented in the shape of graphite sheets with an irregular arrangement.

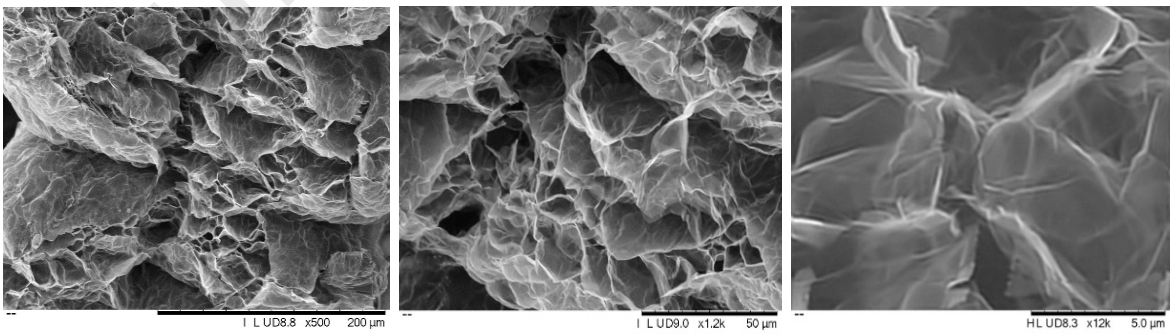

(a) **(b)** **(c)**

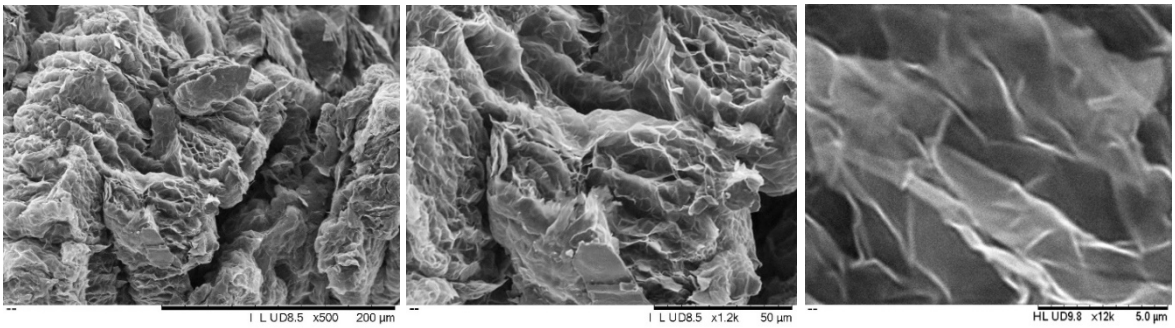

(d) **(e)** **(f)**

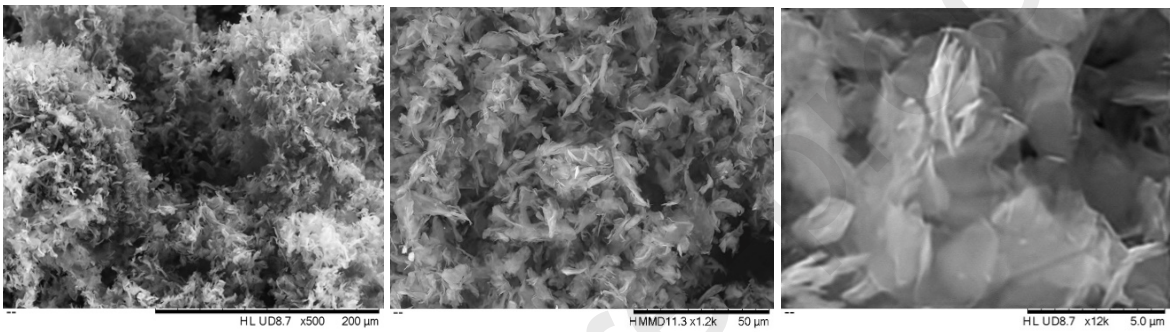

(g) **(h)** **(i)**

Figure 4 Pores of varied sizes on the surface of infiltrated EG1, EG2 and EG3 particles. (a) EG1 (× 500) (b) EG1 (× 1200) (c) EG1 (× 12000); (d) EG2 (× 500) (e) EG2 (× 1200) (f) EG2 (× 12000); (g) EG3 (× 500) (h) EG3 (× 1200) (i) EG3 (× 12000)

Continually zooming on the surface of EG1 and EG2, as shown in Figure 4, pores with varied sizes in a range of 1-60 μm were observed. These pores intersected with each other, formed an irregular networking structure. However, when the particle size of EG reduced to the small micrometre scale (i.e. EG3), there was lack of the connected networking structure, particles were primarily in the form of loose graphite sheets, see Figure 4 (g, h and i).

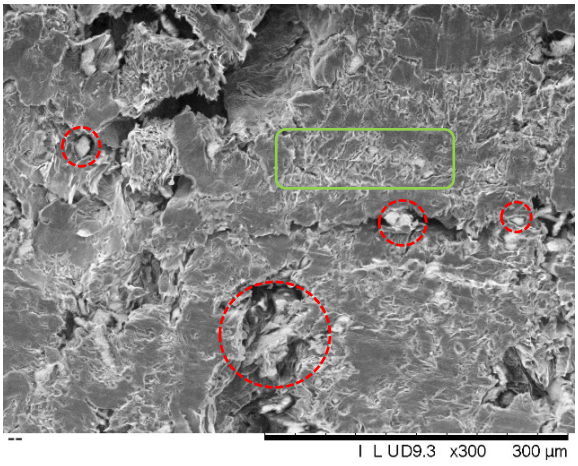

(a)

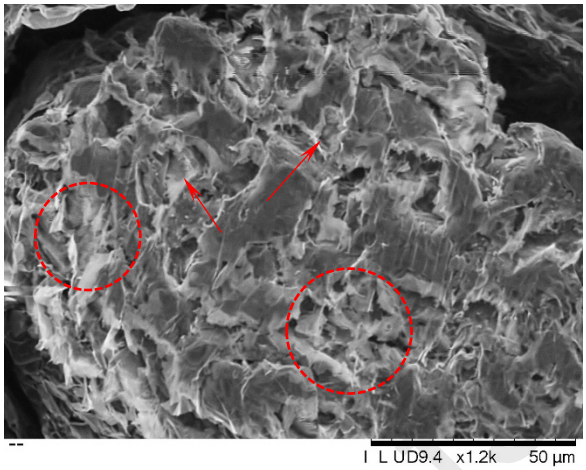

(b)

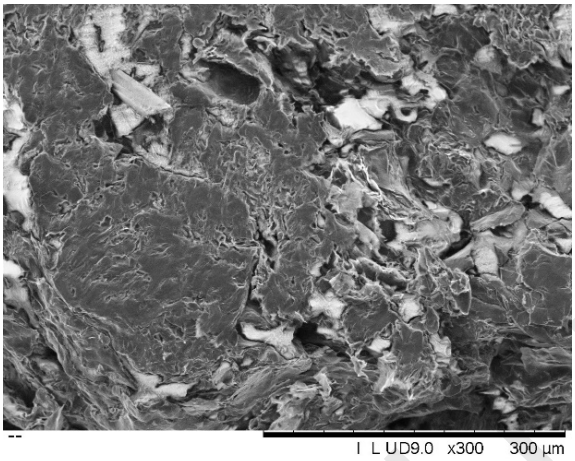

(c)

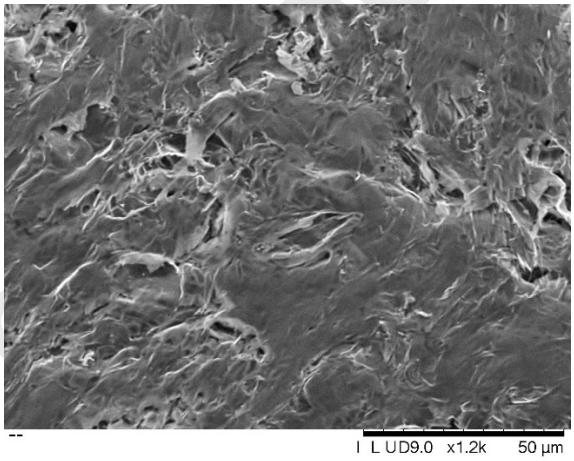

(d)

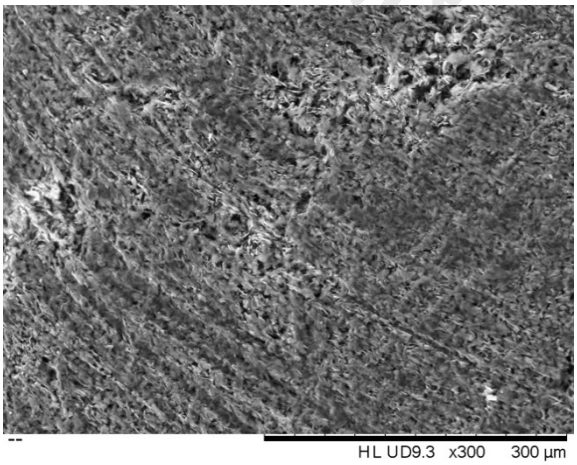

(e)

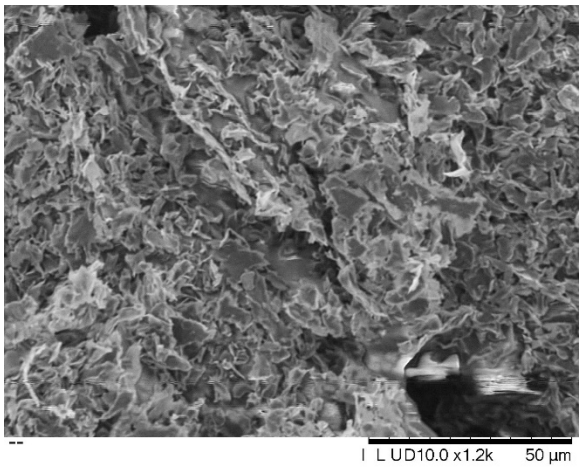

(f)

Figure 5 Cut surfaces of composites at different magnification. Light area- RT28HC, Dark area- EG (a) EG1 Composite, × 300. (b) EG1 Composite, × 1200. (c) EG2

Composite, × 300. (d) EG2 Composite, × 1200. (e) EG3 Composite, × 300. (f) EG3 Composite, × 1200.

Figure 5 presents the cut surfaces of the composite tablets based on the different type of EGs. Paraffin exhibited good compatibility with EG and when paraffin is confined in the graphite pores interaction could be observed between the paraffin and graphite layer. Patrik et al. [24] carried out detailed X-ray diffraction study on low-density polyethene, paraffin and expanded graphite composites. The results proved the partial intercalation of the paraffin wax chains between the graphite layers. The highest intercalation was observed with the highest amount of EG and paraffin wax. The existence of the various pore sizes on the EG matrix, especially of EG1 and EG2, contribute to the adsorption of most of the paraffin.

These different structural arrangements of EG had a great impact on paraffin adsorptions. The SEM pictures (Figure 5) illustrate that composites based on EG1 and EG2 revealed different adsorption behaviours towards paraffin, compare with composite based on EG3. In the case of composites based on EG1 and EG2, paraffin was absorbed into large pores and the gaps built among EG particles, crystallised and aggregated into big particles (see Figure 5 a and c). In addition to this, owing to the capillary force, a mass of the paraffin was retained in relatively small pores of the networking structure. In these circumstances, the morphology of paraffin appeared as needle shapes as indicated in the green area of Figure 5 a. Moreover, the paraffin can be easily impregnated into the void and pore structures of the large micrometre scale EG, also due to the high wetting ability of paraffin in the liquid phase. Li et al. [25] carried out observation on the EG with 180 μm size and found a large number of microvoids on the EG. The voids are constituted by parallel and collapsed layers which were concluded to be the key reason for EG’ s excellent adsorption.

On the contrary, by the reason of lacking the compact networking structure, therefore the capability of the adsorption reduced a great extent. Only a small amount of the PCM was confined in the voids formed among loosed EG3 particles. Most of the paraffin sit on the surface of graphite sheets, so largely white colour can be seen in Figure 5 (e) and (f).

The compact networking structure of EG1 and EG2 matrixes provided good thermal behaviour to the composite. While in the case of EG3 composites, interfacial thermal resistance existed among the small particles, which hinders the heat transfer among the composites. Subsequently, the phase change temperature, thermal conductivity and thermal degradation temperature were

affected by the structure, which will be discussed in the following chapters.

3.1.2 3D structural characterization of the pure EG matrix and paraffin/EG composites.

Pure EG matrix based on different particle sizes were imaged in 3D using a Nano-CT system (XRT). Porosity and specific surface area of EG matrixes were obtained from the 3D binary images (see Table 3). It was found that EG1 and EG2 have relatively large porosity and specific area compared with EG3.

Table 3 Structure parameters of the pure EG matrix.

Material	Porosity (%)	Specific area (1/mm)
EG1	38.01	13.07
EG2	30.06	11.86
EG3	18.03	9.04

The pore size distribution of different pure EG matrixes before the adsorption is shown in Figure 6 (a). It illustrates that EG3 had relatively narrow porosity distribution. The pore size of EG3 was also relatively small, sitting within 27-180 μm. The pore size of EG1 and EG2 mainly located in the range of 135 - 243 μm which was relatively larger than the EG3 matrix. The latter one mostly consists of small particles without significant compact pore structure. These small particles loosely arranged to form unconnected voids (see Figure 4 g-i), the void size was relatively small, compared with the porous structure in EG1 and EG2 matrix. The conclusion can be also confirmed by SEM pictures. EG/paraffin composites were also studied preliminarily. The 3D surface-rendered models were shown in Figure 6 (b). Different material components were visualised in a different colour according to material density (x-ray opacity). In this study, the brown colour indicates low density which is EG, blue colour indicates high density which is paraffin. The results demonstrate the impact of particle size on the EG matrix/PCM adsorption. The pronounced colour difference illustrates that EG matrixes with the connected porous structure have a better capability on PCM adsorption and confinement. EG1 and EG2 have connected pore structure, and PCM are confined in the pores of EG, hence few blue colours are observed at the cross-section of the 3D model. However, in the case of composite with EG3, PCM is not reserved in pores and it is held in the void between small EG

particles. The cross-section of the 3D model almost consists of blue colour which is paraffin, and it indicates the bad adsorption of paraffin into EG.

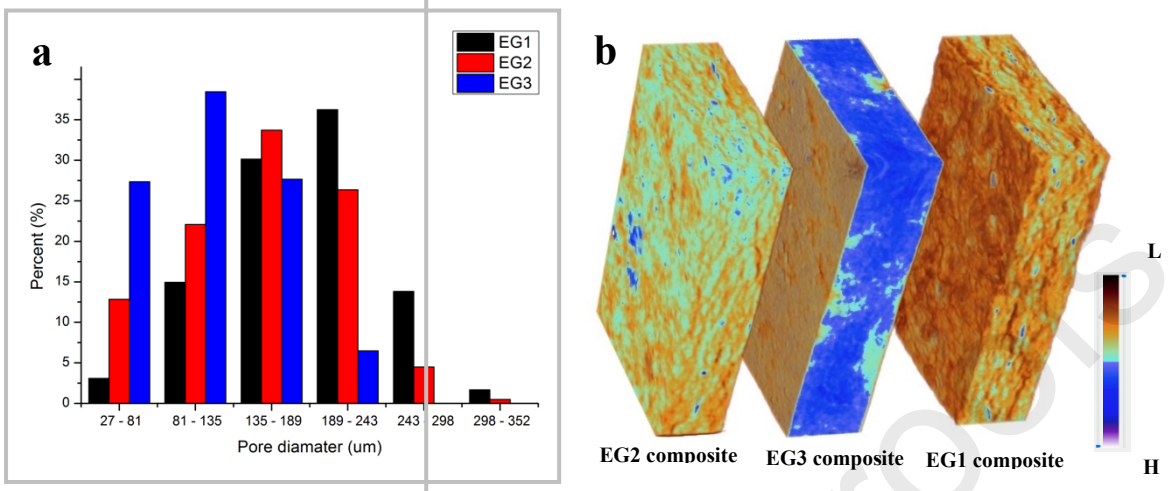

Figure 6 (a) Pore size distribution of EG matrixes, calculated from the binary images (b) 3d surface-rendered models of the cross-section of EG/Paraffin composite with 25wt% of EG loading (brown to blue scale bar indicates the density changing from low to high).

3.2 Thermal characterization

3.2.1 Phase change behaviour study

The phase change temperature of the composites was affected by both thermal conductivity and the porous structure of the EG in a complex manner. In this paper melting peak temperature ($T_{p,m}$) and solidification peak temperature ($T_{p,s}$) are chosen for studying the melting and solidification behaviours of the composites.

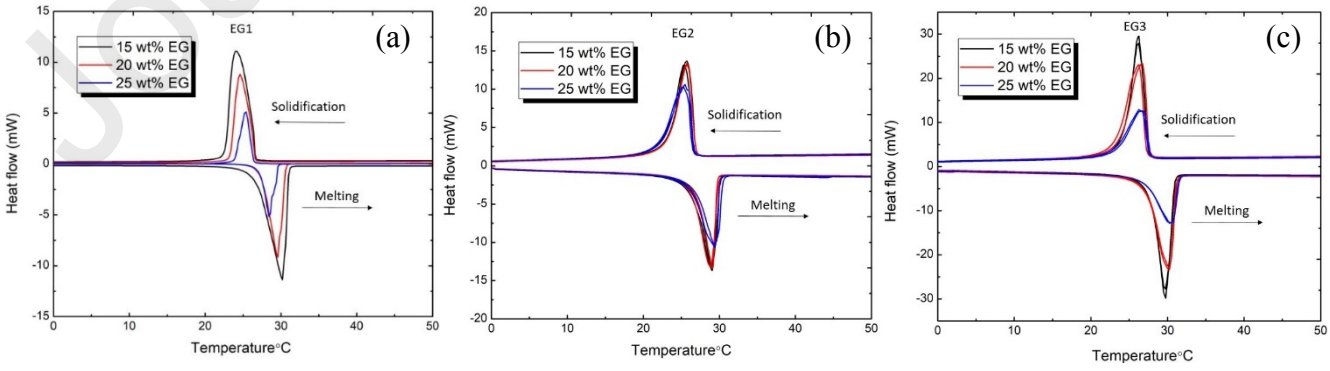

Figure 7 DSC scanning curve for EG based composites. (a) EG1 based composites (b) EG2 based composites (c) EG3 based composites

In Figure 7, the DSC result of the composites displays the well-defined peaks which are associated with the melting and solidification events. The position of the peak varies with the different mass content of EG.

Table 4 Characteristic temperatures obtained from DSC measurement

Material		$T_{p,m}$ (°C)	$T_{p,s}$ (°C)	ΔT= $T_{p,m}$-$T_{p,s}$
EG1	15wt%	29.9	24.33	5.57
	20wt%	29.45	24.77	4.68
	25wt%	28.32	25.48	2.84
EG2	15wt%	28.85	23.31	5.54
	20wt%	28.38	24.62	3.76
	25wt%	28.16	24.75	3.41
EG3	15wt%	28.19	25.79	2.4
	20wt%	28.17	26.34	1.83
	25wt%	28.16	25.72	2.44
RT28HC		28.02	26.24	1.78

Table 4 gives the characteristics temperatures obtained and derived from the DSC measurements. It was found that the maximum difference of $T_{p,m}$ and $T_{p,s}$ between the composites and the raw PCM can reach 1.88 and 2.93 °C, respectively. The $T_{p,m}$ of both EG1 and EG2 based composites was increased comparing with pure RT28HC. In contrast to the $T_{p,m}$, the shift of the $T_{p,s}$ of EG1 and EG2 from bulk RT28HC were negative. Pronounced hysteresis between solidification and melting were observed on the present of EG content. The temperature difference (ΔT) of $T_{p,m}$ and $T_{p,s}$ of the composites were increased by up to 3.79 °C, compared with the raw material. The shift on the phase change temperature of the PCM was also observed by some other researchers [26–28].

The phase change behaviour of PCM confined in pores is influenced by the pore pressure. It could be explained by the Clausius-Clapeyron equation:

$$\frac{dP}{dT} = \frac{L}{T\Delta V}$$

where $\frac{dP}{dT}$ is the slope of the tangent to the coexistence curve at any point which is positive for most PCMs, L is the specific latent heat, T is the temperature, ΔV is the specific volume change of the phase transition.

In the case of RT28HC, L is 220 kJ/ kg, T is 301K and ΔV is roughly 10%. It brings to a positive value of $\frac{dP}{dT}$. The increased volume of the PCM during the solid to liquid phase transition led to increased pressure in the matrix, which in turn results in increasing melting temperature. Similarly, the solidification process of the PCM was influenced by the confinement condition. The decreased volume of PCMs during the solidification led to a decreased pressure, therefore led to a decrease in the solidification temperature.

Moreover, the change of the phase change behaviour could also be affected by the interface between the PCM surface and the pore surface. Alkane form solid adsorbed monolayers at a graphite surface, which lead to the interfacial phenomena of adhesion. The strong interaction between the PCM surface and pore surface resulted in elevated melting temperature and depressed solidification temperature.

The structure of the confined PCM is relevant to determinate the melting and freezing temperature. As it was observed in this study, EG matrix has a tight network structure. The pore networking effect influenced the hysteresis. The interconnected pores affect the melting and solidification of the PCM and cause larger hysteresis, leading to different property unlike that of pure PCM.

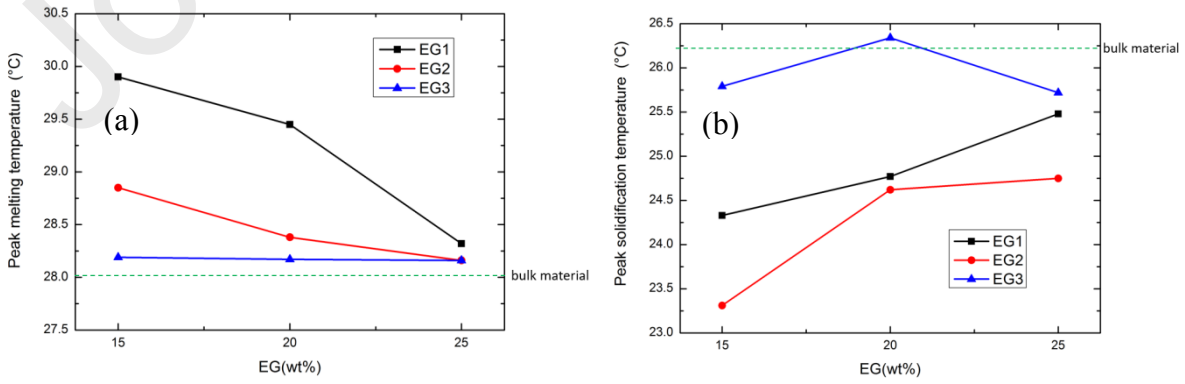

Figure 8 Melting and solidification peak temperatures of EG based composites in comparison with the bulk PCM

The morphology of EG was not the only factor that affected the phase change temperature of the PCM. Figure 8 illustrates the impact of the EG amount on the PCM phase change behaviour. The melting temperature of the EG1 and EG2 based composites decreased with the increase of EG mass percentage so that composites with 25wt% EG content had the lowest $T_{p,m}$, and the value was close to the $T_{p,m}$ of the raw material. The $T_{p,s}$ in this case was increasing with the increased mass percentage of EG. $T_{p,s}$ of composites with 25wt% EG content was also close to the $T_{p,s}$ of the raw material. Hence the hysteresis of EG1 and EG2 based composites were reduced with more EG content.

The difference in the thermal conductivity of composites results in the differences discussed above. Increased EG content improved the thermal conductivity of composites, and it strengthens the heat transfer among the composites. In the case of solidification, heterogeneous nucleation of the PCM was also benefited from the increased EG content.

The $T_{p,m}$ and $T_{p,s}$ of EG3 based composites were not observed with an obvious phase change temperature alteration behaviour. As indicated in the SEM study (see Figure 4 and Figure 5), EG3 did not appear like a complex networking structure because of the small particle size. Although a limited number of micro-pores (~15μm) still existed among the EG3 particles, it had an insignificant impact on the phase change behaviour of the PCM.

3.2.2 Latent heat and specific heat study

Table 5 demonstrates that the latent heat and specific heat of the composite were affected by the different mass percentage of EG. Latent heat (Δh) was obtained by the integration of the area between the peak and an extrapolated based line. The results of the latent heat measurement of the EG composites with different mass percentage are shown in Figure 9 and Table 5.

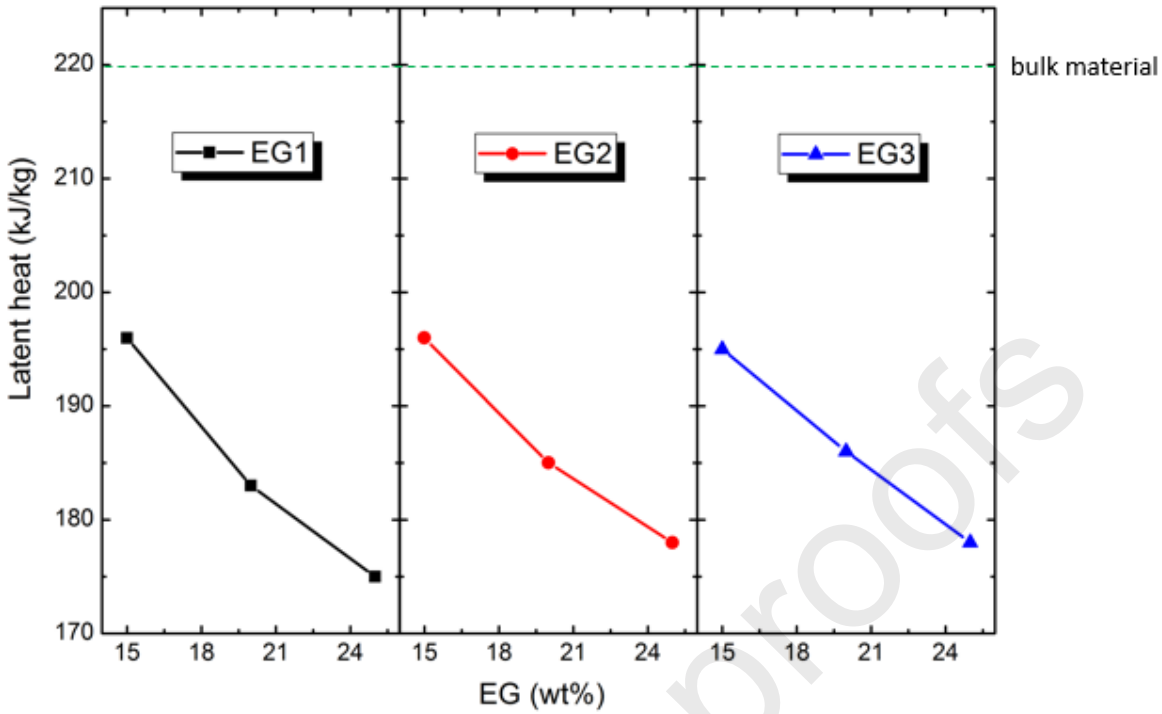

Figure 9 Variation of latent heat versus EG mass percentage at different EG particle size

Table 5 Latent heat and the specific heat (of both liquid and solid phases) of composites obtained from the DSC measurements

Material		Latent heat (kJ/kg)	Solid state specific heat	Liquid state specific heat
EG1	15wt%	196 ± 1.47	1.16	2.13
	20wt%	183 ± 1.15	0.88	1.79
	25wt%	175 ± 1.73	0.76	1.12
EG2	15wt%	196 ± 0.75	2.19	2.81
	20wt%	189 ± 1.00	1.83	2.35
	25wt%	178 ± 1.14	1.79	2.1
EG3	15wt%	195 ± 1.48	1.65	1.92

20wt%	186 ± 0.84	1.52	1.91
25wt%	178 ± 1.53	1.43	1.82

The latent heat of composites was inversely proportional to the EG content, which decreased by 5% with the 5wt% increase of EG content.

The results of the specific heat of the composites are also displayed in Table 5. The specific heat of EG in the range of 0.47 ~ 0.65 kJ/(kg K) at ambient temperature [29], while RT28HC has a specific heat of 2 kJ/(kg K) at the same condition. With more EG presented, the specific heat of the composite decreased as EG has a lower specific heat than the RT28HC.

3.2.3 Thermal stability study

The thermal stabilities of the composites with different mass percentage and different particle size of EG were evaluated by TG analysis. In this paper, the onset degradation temperature ($T_{on,d}$) and peak degradation temperature ($T_{p,d}$) were chosen as the criteria for studying the thermal characteristics of the composites. As shown in Figure 10 (a), extrapolated onset temperature ($T_{on,d}$) indicated the beginning of the weight loss and the peak degradation temperature ($T_{p,d}$) was the point that has the greatest changing rate on weight loss.

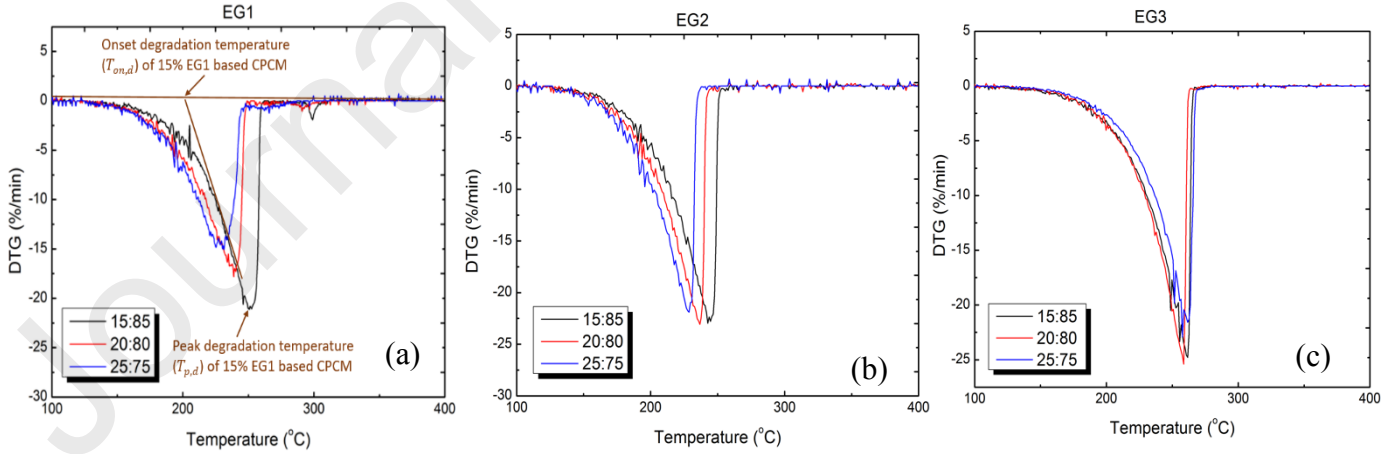

Figure 10 DTG curve for EG based composites. (a)EG1 based composites (b)EG2 based composites (c)EG3 based composites

The derivative thermogravimetry (DTG) result of the composites is shown in Figure 10. The degradation temperatures and the charred residue amount after the degradation are shown in Table 6.

Table 6 Thermal stability properties obtained from the DTG curve ($T_{on,d}$ is onset degradation temperature, $T_{p,d}$ is the peak degradation temperature)

Materials		$T_{on,d}$ (°C)	$T_{p,d}$ (°C)	Charred residue (%)
EG1	15wt%	219	251	16.40
	20wt%	205	234	19.96
	25wt%	196	231	27.15
EG2	15wt%	212	243	15.98
	20wt%	207	237	21.66
	25wt%	199	229	25.60
EG3	15wt%	227	255	14.83
	20wt%	227	255	19.55
	25wt%	230	257	25.91
RT28HC		196	220	0.38

It can be seen from Figure 10 that the thermal degradation process completed in one step for all composites, corresponding to the degradation of RT28HC. A larger amount of the charred residues was observed from measurements of the composite with more weight percentage of EG content. Because of the degradation temperature of EG is more than 800 °C. Besides, the charred amount was almost consistent with the EG content of the corresponding composite. Therefore, the residue from the degradation tests was mainly EG.

$T_{on,d}$ and $T_{p,d}$ were influenced by the particle size and mass percentage of the EG. The $T_{on,d}$ and $T_{p,d}$ of RT28HC are 196°C and 220°C, respectively. It could be observed from the results that EG had a positive effect on the degradation of composites, leading to a significant increase in the degradation temperatures. The maximum increase in the $T_{on,d}$ of composites were 34 °C comparing with RT28HC. The increase in $T_{p,d}$ of the composites obtained in the range of 9-37 °C

Figure 10 and Table 6 can conclude that the existence of EG had a great contribution to the thermal stability of the composites. In the case of EG with the large particle size (i.e. EG1 and EG2), the PCM was confined in the pores on EG particles. The porous structure on the EG particles was therefore advantageous for slowing the escape of the volatile products generated during thermal degradation. Hence it hindered the degradation process and improved the thermal stability of the composites. Although EG3 with small particle size has an unconnected porous structure, it also increased the degradation temperature of the composites and had a positive effect on the thermal stability. The fine EG particles built matrix that could also help with the escape of the paraffin vapour. Interfacial thermal resistance dominated the heat transfer in the composite, which further increased the thermal degradation temperature.

The amount of EG content played a role in the degradation temperatures. In the case of EG1 and EG2 based composites, a higher weight percentage of EG led to a lower thermal degradation temperature. When comparing the composites at the different mass percentage of EG1, 23°C and 20 °C of difference were observed on the $T_{on,d}$ and $T_{p,d}$, respectively. The difference between the $T_{on,d}$ and $T_{p,d}$ was 13 °C and 14 °C in the case of EG2 based composites, respectively. With a higher mass percentage of the EG content, the thermal conductivity of the composites was improved. In such a way, it strengthened the heat transfer inside the composite, thus led to attaining a lower degradation temperature. Composites contained EG3 were not observed with a significant difference in the degradation temperatures.

3.2.4 Leakage study

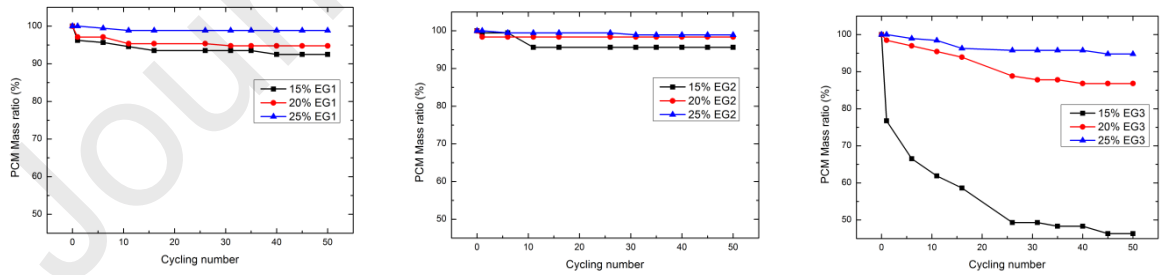

(a) (b) (c)

Figure 11 PCM mass ratio change after 50 thermal cyclings. (a)EG1 based composites (b)EG2 based composites (c)EG3 based composites

The leakage phenomena of the composites was also studied through thermal cycling the samples. Figure 11 shows the mass ratio change of the PCM in the composites based on EG 1,

EG2 and EG3 with 10%, 15% and 25 wt% EG after 50 thermal cyclings. It can be indicated from the results that the most pronounced leakage occurred in EG3 composite using 15 wt% EG. After the first cycling, 24 wt% of PCM leaked from the composite and the leakage then continued at a rate of 5 wt% PCM/5 cycle until 25 cycles. The PCM leakage within the EG3 composites was improved when the mass ratio of EG was improved. After 50 cycles EG3 composite with 20 wt% EG remained 87 wt% PCM, and EG3 composite with 25 wt% EG was not observed with significant leakage.

Regarding the composites using large particle size EG, the composites containing 20 wt% and 25 wt% EG was observed to be form stable as after 50 cycles there was less than 5 wt% PCM leakage. The composites with 15 wt% large particle EG has slightly worse cycling stability and 15 wt% EG1 composite and 15 wt% EG2 composite were found to have 8 wt% and 6 wt% PCM leakage after 50 cycles, respectively.

From the results, it can be concluded that the mass ratio of EG is the determining factor for the cycling stability of EG based composites. After 50 cycles the weight of PCM remained in the composites with 20 wt% and 25 wt% large particle size EG were maintained nearly constant, and the leakage was significantly reduced when the mass ratio of EG3 in the composite was improved to 20 % and 25 %. Particle size is another factor which influences the composite cycling stability. Comparing EG3 with EG1, after 50 cycles the remaining PCM mass ratio of EG3 was 46 %, 8 wt% and 4 wt% less than EG1 with 15 wt%, 20 wt% and 25 wt% EG content, respectively. The difference between the composites using different particle size EG is due to the different EG structure. Large EG particles have pores and voids which are able to confine the PCM, while small EG particles are lack of pore structure and are not able to preserve PCM.

3.2.5 Thermal conductivity study

The thermal conductivity result of composites with different mass percentage and different particle size of EG is shown in Figure 12 and Table 7.

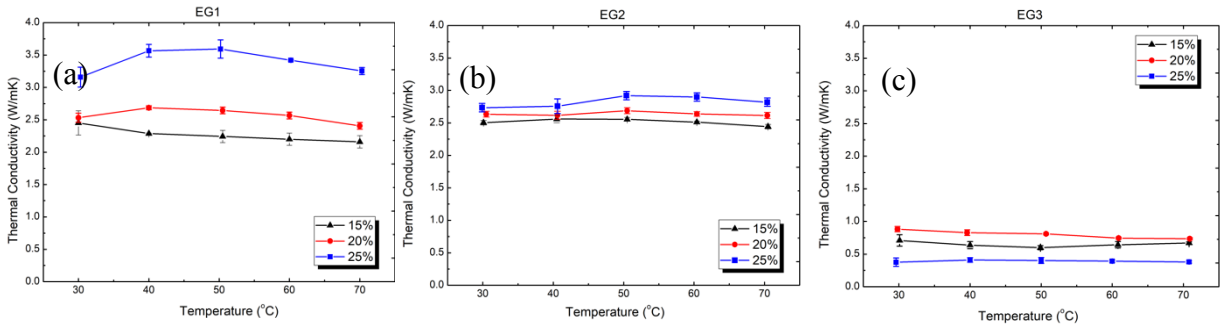

Figure 12 Thermal conductivity of solid and liquid phases as a function of temperature. (a) EG1 EG based composites (b) EG2 EG based composites (c) EG3 EG based composites

With the present of EG, the thermal conductivity of the composites was improved effectively. The larger particle size of the EG had a more pronounced effect on the thermal conductivity of the composites. The thermal conductivity of the composites increases in the order of EG1≈EG2> EG3. For instance, with 25wt% of EG loading, EG1, EG2 and EG3 composites had a thermal conductivity of 3.16, 2.74 and 0.38 W/mK at 30 °C, respectively. Regarding the large micrometres scale EG, the thermal conductivity increased with the EG loading. However, in the case of EG3 presented, the rising tendency was unnoticeable. The decreased thermal conductivity with decreased particle size can be attributed to the effect of interfacial thermal resistance. When the particle is small, the interfacial thermal resistance would dominate the influence on thermal conductivity of the composite. Nevertheless, if the particle size is relatively large, the thermal conductivity of the composites was decided by the bulk property. In Figure 12 (c), the sudden drop in the thermal conductivity of the EG3 composites suggests there was a significant interfacial thermal resistance among the small graphite particles.

Table 7 Thermal conductivity data obtained from the LFA measurement.

		Thermal conductivity (W/mK)				
Material		30°C	40°C	50°C	60°C	70°C
EG1	15wt%	2.45 ± 0.19	2.29 ± 0.01	2.24 ± 0.09	2.20 ± 0.09	2.16 ± 0.09
	20wt%	2.53 ± 0.07	2.69 ± 0.03	2.64 ± 0.05	2.57 ± 0.05	2.41 ± 0.05
	25wt%	3.16 ± 0.15	3.57 ± 0.10	3.59 ± 0.14	3.42 ± 0.01	3.25 ± 0.06

	15wt%	2.50 ± 0.03	2.56 ± 0.06	2.56 ± 0.03	2.51 ± 0.02	2.44 ± 0.03
EG2	20wt%	2.64 ± 0.04	2.62 ± 0.06	2.69 ± 0.05	2.64 ± 0.04	2.62 ± 0.05
	25wt%	2.74 ± 0.06	2.76 ± 0.11	2.92 ± 0.07	2.90 ± 0.06	2.82 ± 0.06
	15wt%	0.71 ± 0.09	0.64 ± 0.06	0.60 ± 0.03	0.64 ± 0.05	0.67 ± 0.02
EG3	20wt%	0.88 ± 0.04	0.83 ± 0.04	0.81 ± 0.02	0.74 ± 0.01	0.74 ± 0.02
	25wt%	0.38 ± 0.06	0.41 ± 0.04	0.40 ± 0.05	0.39 ± 0.02	0.38 ± 0.02

In this study, the two-form Maxwell-Eucken model was also used for theoretically predicting the thermal conductivity of EG composites. The model is defined as following [30]:

$$K = \frac{k_1 v_1 + k_2 v_2 \dfrac{3k_1}{2k_1 + k_2}}{v_1 + v_2 \dfrac{3k_1}{2k_1 + k_2}}$$

Where K is the effective thermal conductivity of the composites, k_1 is the thermal conductivity of the continuous phase (EG), v_1 is the volume fraction of the continuous phase, k_2 is the thermal conductivity of the dispersed phase (paraffin), v_2 is the volume fraction of the dispersed phase.

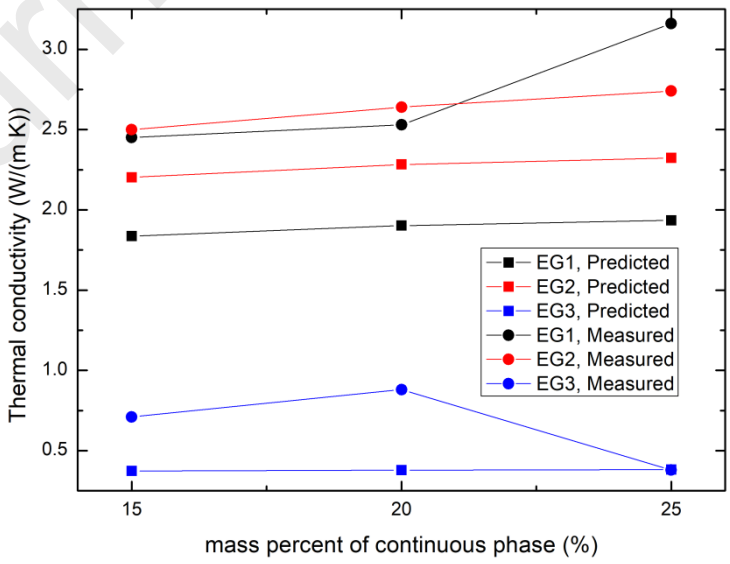

Figure 13 A comparison between the theoretical predictions and experimental measured thermal conductivities of EG composites.

The thermal conductivity of pure EG1, EG2 and EG3 matrix was measured to be 3.23, 3.92 and 0.5 W/mK, respectively. Xia et al. [27] observed the distribution of EG in the EG/PCM composite using a polarizing optical microscope and found out that EG matrix forms a continuous phase when the mass percentage of EG in the composite is more than 4%. In this study, the mass fraction of the EG was more than 15wt%, hence the EG matrix presented as the continuous phase, and RT28HC was the dispersed phase. It can also be observed from the SEM picture of the cut surface of composites that EG matrix existed continuously. The volume fraction of the continuous phase was achieved from the measured value. The volume fraction of the dispersed phase was calculated from the weight and density of the dispersed phase at solid-state. The predicated data is shown in Figure 13. The results show that the predicted data has good agreement with experimental data.

4. Conclusion

It has been observed that EG particles with different particle size have different structures, results in dissimilarities on EG matrix structures. SEM pictures showed that large EG particles (i.e. EG1 and EG2) with loose vermicular shape possessed interconnected pore structure, while the small EG particles (i.e. EG3) was primarily in the form of loose graphite sheets without connected networking structure. 3D structure characterization revealed that large EG matrix had higher porosity and higher pore/void size comparing with the small EG matrix. Different structural arrangements of EG had a great impact on paraffin adsorptions, hence affects the thermal behaviour of EG/paraffin composites.

The interconnected pore structure of large EG matrix confined PCM in the pores and voids and led to an increased temperature hysteresis comparing with the pure paraffin. The pore structure of the large EG matrix could help with confining the EG and it had advantageous in slowing the escape of the volatile products generated during thermal degradation. The confinement behaviour was further confirmed in the thermal cycling test. The test showed composites using large particle size EG has a significantly lower PCM loss than composites using small size EG. It was also revealed that the mass ratio of the EG content is the determining factor of the composite cycling stability. Thermal stability of composites containing large EG particles was effectively improved as indicated by the results from TG analysis. The thermal conductivity of

composites with large EG particles increased by 1360% - 1695% because of the high thermal conductivity of the EG matrix. In the case of small EG particles, interfacial thermal resistance dominates the influence on thermal conductivity, which results in less improvement in thermal conductivity. A 90 ~ 340% increment on thermal conductivity was obtained regarding different EG contents. Interfacial thermal resistance also helped with improving the thermal stability of the composite.

Acknowledgements

The research was supported by the Global Energy Interconnection Research Institute Europe GmbH through Agreement number SGRIKXJSKF[2017]632. Any finding, conclusion, opinions expressed in this article are those of the authors and do not necessarily reflect the views of the Global Energy Interconnection Research Institute Europe GmbH.

References

[1] K. Pielichowska, K. Pielichowski, Phase change materials for thermal energy storage, Progress in Materials Science. 65 (2014) 67–123. doi:https://doi.org/10.1016/j.pmatsci.2014.03.005.

[2] A. Mills, M. Farid, J.R. Selman, S. Al-Hallaj, Thermal conductivity enhancement of phase change materials using a graphite matrix, Applied Thermal Engineering. 26 (2006) 1652–1661. doi:10.1016/j.applthermaleng.2005.11.022.

[3] Z. Wang, Z. Zhang, L. Jia, L. Yang, Paraffin and paraffin/aluminum foam composite phase change material heat storage experimental study based on thermal management of Li-ion battery, Applied Thermal Engineering. 78 (2015) 428–436. doi:10.1016/j.applthermaleng.2015.01.009.

[4] A. Babapoor, M. Azizi, G. Karimi, Thermal management of a Li-ion battery using carbon fiber-PCM composites, Applied Thermal Engineering. 82 (2015) 281–290. doi:10.1016/j.applthermaleng.2015.02.068.

[5] Y. Azizi, S.M. Sadrameli, Thermal management of a LiFePO4 battery pack at high temperature environment using a composite of phase change materials and aluminum wire mesh plates, Energy Conversion and Management. 128 (2016) 294–302. doi:10.1016/j.enconman.2016.09.081.

[6] S. Ramakrishnan, X. Wang, J. Sanjayan, Effects of various carbon additives on the thermal storage performance of form-stable PCM integrated cementitious composites, Applied Thermal Engineering. 148 (2019) 491–501. doi:https://doi.org/10.1016/j.applthermaleng.2018.11.025.

[7] A. Sarı, A. Bicer, F.A. Al-Sulaiman, A. Karaipekli, V. V Tyagi, Diatomite/CNTs/PEG composite PCMs with shape-stabilized and improved thermal conductivity: Preparation and thermal energy storage properties, Energy and Buildings. 164 (2018) 166–175. doi:https://doi.org/10.1016/j.enbuild.2018.01.009.

[8] A. Sarı, A. Al-Ahmed, A. Bicer, F.A. Al-Sulaiman, G. Hekimoğlu, Investigation of thermal properties and enhanced energy storage/release performance of silica fume/myristic acid composite doped with carbon nanotubes, Renewable Energy. 140 (2019) 779–788. doi:https://doi.org/10.1016/j.renene.2019.03.102.

[9] M. Chirtoc, N. Horny, I. Tavman, A. Turgut, I. Kökey, M. Omastová, Preparation and photothermal characterization of nanocomposites based on high density polyethylene filled with expanded and unexpanded graphite: Particle size and shape effects, International Journal of Thermal Sciences. 62 (2012) 50–55. doi:https://doi.org/10.1016/j.ijthermalsci.2012.02.015.

[10] G. Jiang, J. Huang, Y. Fu, M. Cao, M. Liu, Thermal optimization of composite phase change material/expanded graphite for Li-ion battery thermal management, Applied Thermal Engineering. 108 (2016) 1119–1125. doi:https://doi.org/10.1016/j.applthermaleng.2016.07.197.

[11] A. Karaipekli, A. Sari, K. Kaygusuz, Thermal conductivity improvement of stearic acid using expanded graphite and carbon fiber for energy storage applications, Renewable Energy. 32 (2007) 2201–2210. doi:10.1016/j.renene.2006.11.011.

[12] A. Sarı, A. Karaipekli, Preparation, thermal properties and thermal reliability of palmitic acid/expanded graphite composite as form-stable PCM for thermal energy storage, Solar Energy Materials and Solar Cells. 93 (2009) 571–576. doi:https://doi.org/10.1016/j.solmat.2008.11.057.

[13] A. Sari, A. Karaipekli, Thermal conductivity and latent heat thermal energy storage

characteristics of paraffin/expanded graphite composite as phase change material, Applied Thermal Engineering. 27 (2007) 1271–1277. doi:10.1016/j.applthermaleng.2006.11.004.

[14] P. Zhang, Y. Hu, L. Song, J. Ni, W. Xing, J. Wang, Effect of expanded graphite on properties of high-density polyethylene/paraffin composite with intumescent flame retardant as a shape-stabilized phase change material, Solar Energy Materials and Solar Cells. 94 (2010) 360–365. doi:10.1016/j.solmat.2009.10.014.

[15] A.G. Every, Y. Tzou, D.P.H. Hasselman, R. Raj, The effect of particle size on the thermal conductivity of ZnS/diamond composites, Acta Metallurgica et Materialia. 40 (1992) 123–129. doi:https://doi.org/10.1016/0956-7151(92)90205-S.

[16] T. Luo, J.R. Lloyd, Enhancement of Thermal Energy Transport Across Graphene/Graphite and Polymer Interfaces: A Molecular Dynamics Study, Advanced Functional Materials. 22 (2012) 2495–2502.

[17] A.G. Every, Y. Tzou, D.P.H. Hasselman, R. Raj, The effect of particle size on the thermal conductivity of ZnS/diamond composites, Acta Metallurgica et Materialia. 40 (1992) 123–129. doi:https://doi.org/10.1016/0956-7151(92)90205-S.

[18] R. RADHAKRISHNAN, K.E. GUBBINS, Free energy studies of freezing in slit pores: an order-parameter approach using Monte Carlo simulation, Molecular Physics. 96 (1999) 1249–1267. doi:10.1080/00268979909483070.

[19] D. Zhang, S. Tian, D. Xiao, Experimental study on the phase change behavior of phase change material confined in pores, Solar Energy. 81 (2007) 653–660. doi:https://doi.org/10.1016/j.solener.2006.08.010.

[20] D.D. Awschalom, J. Warnock, Supercooled liquids and solids in porous glass, Physical Review B. 35 (1987) 6779–6785. doi:10.1103/PhysRevB.35.6779.

[21] L.W. Wang, Z. Tamainot-Telto, S.J. Metcalf, R.E. Critoph, R.Z. Wang, Anisotropic thermal conductivity and permeability of compacted expanded natural graphite, Applied Thermal Engineering. 30 (2010) 1805–1811. doi:https://doi.org/10.1016/j.applthermaleng.2010.04.014.

[22] mettler toledo, Heat Capacity, (2019). https://www.mt.com/gb/en/home/perm-lp/product-organizations/ana/TA-Cp_specific_heat_capacity.html (accessed December 19, 2019).

[23] P. Sobolčiak, H. Abdelrazeq, M. Ouederni, M. Karkri, M.A. Al-Maadeed, I. Krupa, The stabilizing effect of expanded graphite on the artificial aging of shape stabilized phase change materials, Polymer Testing. 46 (2015) 65–71. doi:https://doi.org/10.1016/j.polymertesting.2015.06.017.

[24] P. Sobolciak, M. Mrlík, M.A. AlMaadeed, I. Krupa, Calorimetric and dynamic mechanical behavior of phase change materials based on paraffin wax supported by expanded graphite, Thermochimica Acta. 617 (2015) 111–119. doi:https://doi.org/10.1016/j.tca.2015.08.026.

[25] Y. Li, H. Yan, Q. Wang, H. Wang, Y. Huang, Structure and thermal properties of decanoic acid/expanded graphite composite phase change materials, Journal of Thermal Analysis and Calorimetry. 128 (2017) 1313–1326. doi:10.1007/s10973-016-6068-4.

[26] D. Zhang, J. Zhou, K. Wu, Z. Li, Granular phase changing composites for thermal energy storage, Solar Energy. 78 (2005) 471–480. doi:https://doi.org/10.1016/j.solener.2004.04.022.

[27] L. Xia, P. Zhang, R.Z. Wang, Preparation and thermal characterization of expanded graphite/paraffin composite phase change material, Carbon. 48 (2010) 2538–2548. doi:https://doi.org/10.1016/j.carbon.2010.03.030.

[28] X. Xiao, P. Zhang, M. Li, Preparation and thermal characterization of paraffin/metal foam composite phase change material, Applied Energy. 112 (2013) 1357–1366. doi:https://doi.org/10.1016/j.apenergy.2013.04.050.

[29] L.L. Vovchenko, L.Y. Matzui, A.A. Kulichenko, Thermal characterization of expanded graphite and its composites, Inorganic Materials. 43 (2007) 597–601. doi:10.1134/S0020168507060088.

[30] J. Wang, J.K. Carson, M.F. North, D.J. Cleland, A new approach to modelling the effective thermal conductivity of heterogeneous materials, International Journal of Heat and Mass Transfer. 49 (2006) 3075–3083.

doi:https://doi.org/10.1016/j.ijheatmasstransfer.2006.02.007.

Declaration of interests

☒ The authors declare that they have no known competing financial interests or personal relationships that could have appeared to influence the work reported in this paper.

☐The authors declare the following financial interests/personal relationships which may be considered as potential competing interests:

- Particle size effect of expanded graphite on the thermal property of expanded graphite/paraffin material was investigated.
- Thermal conductivity enhancement of up to 1695% was observed in large particle size expanded graphite/paraffin material compared with the paraffin PCM.
- After 50 cycles less than 5wt% PCM leakage was found in large particle size expanded graphite/paraffin material.
- A higher degradation temperature with up to 37 °C increase was observed for the composite containing small EG particles when compared with the paraffin PCM.